Article

A Theoretical and Experimental Study of Cysteine-Based Perfluorinated Derivatives

Sisa Chalán-Gualán[1], Iván Ramos-Tomillero[2], Thibault Terencio[1], Lola De Lima[1], Daniela G. Navas-León[1], Nelson Santiago Vispo[3], Fernando Albericio[2,4,5,6] and Hortensia Rodríguez [1,*]

1   School of Chemical Science and Engineering, Yachay Tech, Yachay City of Knowledge, Urcuqui, Ecuador.; sisa.chalan@yachaytech.edu.ec, tthibault@yachaytech.edu.ec, ldelima@yachaytech.edu.ec, dnavas@yachaytech.edu.ec, hmrodriguez@yachaytech.edu.ec
2   CIBER-BBN, Networking Centre of Bioengineering, Biomaterials, and Nanomedicine.
3   School of Biological Science and Engineering, Yachay Tech, Yachay City of Knowledge, Urcuqui, Ecuador.; nvispo@yachaytech.edu.ec
4   Department of Organic Chemistry, University of Barcelona and CIBER-BBN, 08028 Barcelona, Spain
5   School of Chemistry and Physics, University of KwaZulu-Natal, Durban 4001, South Africa. Albericio@ukzn.ac.za

6   ***** Correspondence: hmrodriguez@yachaytech.edu.ec (H.R.); +593-994-336-513 (H.R.)

Abstract: A series of cysteine-based perfluoroaromatic (hexafluorobenzene (**I**) and decafluorobiphenyl (**II**) were synthesized and established as a chemoselective and available core to simple or more complex systems since small molecules to biomolecules with interesting properties. As proof of concept of the potential application of perfluorinated derivatives as non-cleavable linkers, some antibody-perfluorinated conjugates were prepared via thiol, demonstrating that the bioconjugation process doesn't affect to the macromolecular entity. Besides, some molecular properties of synthesized compounds are evaluated using a combination of spectroscopic characterization (FT-IR and ^{19}F-NMR chemical shifts) and theoretical calculations. Moreover, molecular Docking was also developed to predict cysteine-based hexafluorobenzene and decafluorobiphenyl derivatives' affinity against topoisomerase Il and cyclooxygenase 2 (COX-2). The results suggested that mainly cysteine-based decafluorobiphenyl derivatives could be potential topoisomerase II α and COX-2 inhibitors, becoming potential anticancer agents and candidates for anti-inflammatory treatment.

Keywords: Perfluorinated derivatives; Nucleophilic Aromatic Substitution; Bioconjugation; IR and ^{19}F-NMR simulations; Molecular Docking

1. Introduction

In nature, chemical modifications occur specifically through a wide envelope of reactive amino acid side chains; thus, the challenge has been mimicking that kind of natural modification for years. An essential parameter in bioconjugation is the regioselectivity achieved over a series of reactive groups such as thiols, amines, alcohols, or carboxylic acids[1].

Various methods have been reported for bioconjugation[2], focusing on using natural amino acids of the biomolecule and modifying it, creating specific sites for bioconjugation. In this context, cysteine (Cys), a natural amino acid, promotes a regioselective bioconjugation in antibodies, proteins, and peptides because it is the less common amino acid among the 20 natural amino acids [3–5]. Cysteine is generally present in biomolecules as a disulfide and needs a previous reduction to create an active thiol group[6,7]. Additionally, this is one of the most effective amino acids that allow for obtaining more homogeneous conjugation, improving the therapeutic index and stability of ADCs [8,9]. The cysteine thiol group is more acid (pKa≈ 8) than any other common nucleophiles found in

biomolecules, and sulfur is more polarizable (soft) than nitrogen or oxygen. These important chemical features make its thiol more reactive than any other protein nucleophiles toward electrophiles like alkyl halides, haloacetyl, and maleimides[10,11].

On the other hand, cysteine-S-perfluoroarylation has been used as a platform to access rigid perfluoroaromatic staples and to suit generic entities with exciting properties. In the 1960s, many research groups developed studies on their reactivity, selectivity, and substitution patterns for perfluoroarenes with thiolates proposing that the reaction goes via nucleophilic aromatic substitution (SNAr)[12–14]. The Pentelute research group evaluated commercial perfluoroaromatic rings (decafluorobiphenyl (DFBP) and hexafluorobenzene (HFB)) with different amino acids using mild conditions reagents[15]. It was found that these simple perfluoroaromatic rings react only with the thiol group of cysteine but not with other nucleophiles of amino acids, and the 1,4-disubstituted regioisomer was exclusively observed. However, the monoarylated product was observed when a larger excess (>10-fold) of hexafluorobenzene /decafluorobiphenyl was added. Further studies found that these perfluoroaromatic rings are efficiently crosslinked with cysteine thiols in unprotected peptides (**Scheme. 1a**). The monosubstituted product is obtained when an excess of the perfluoroarene was added (**Scheme. 1b**).
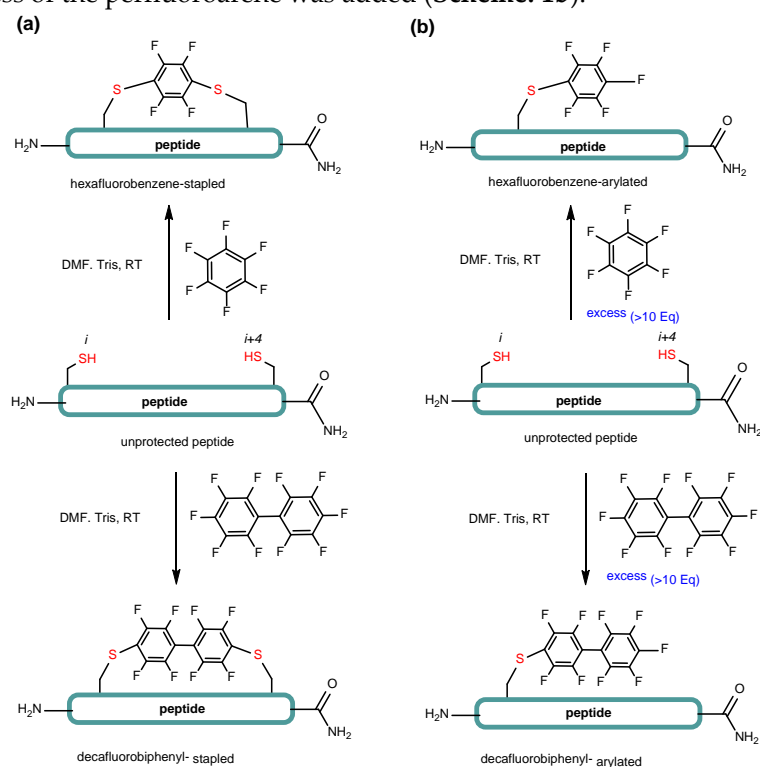
Scheme 1. First generation of perfluoroaromatics linkers: hexafluorobenzene (HFB) and decafluorobiphenyl (DFBP) for peptide modification. (a) Peptide stapling with HFB and DFBP and (b) Peptides arylation employing >10 eq of perfluoroaromatics compounds

Furthermore, they report a successful macrocyclization for relatively short peptides (14 amino acid residues), but for longer peptides, it becomes inefficient because of the large entropic penalty[16]. Additionally, they study the enzymatic site-specific Cys perfluoroarylation for peptides like glutathione (GSH), which have the following sequence, γ-Glu-Cys-Gly45. This work mentioned that arylation of perfluoroaromatic molecules fulfills some "click chemistry" requirements, making them potentially attractive non-cleavable linkers for further bioconjugations. Additionally, HFB and DFBP were employed for more complex systems such as ADCs and protein modifications through a π-clamp (Phe-Cys-Pro-Phe) which can tune the reactivity of its Cys thiol and a reactive peptide interface (RPI) sequence [17,18].

In drug development, density functional theory (DFT) and molecular docking analysis help to complement laboratory research allowing the foretelling of physical and chemical properties and even predicting or confirming biological activity[19].

As a part of the continuing interest in studying perfluoroaromatic scaffolds, herein, we carried out a theoretical and experimental study of cysteine-based perfluorinated derivatives. In this regard, the synthesis and characterization of cysteine-based hexafluorobenzyl and decafluorobiphenyl derivatives (**Ia-b**, and **IIa-c**) were optimized. In the same way, some strategies for bioconjugation were tested to demonstrate the feasibility of these scaffolds as non-cleavable linkers. Besides, theoretical studies were developed to deepen the molecular properties of cysteine-based perfluorinated compounds (**Ia-b**, and **IIa-b**). Additionally, a molecular docking simulation has been carried out using topoisomerase Il and cyclooxygenase 2 (COX-2) as receptors to estimate the potential application of these derivatives as anticancer or anti-inflammatory agents, respectively.

2. Results

2.1. Experimental approach to monosubstituted-perfluoroaromatic derivatives

2.1.1. Perfluoroaromatic scaffolds

The perfuoroarylated HFB (**I**) and DFBF (**II**) were bonded to cysteine (Cys, 1 eq) and to reduced glutathione (GSH, 1 eq), which contains an available thiol group in their structure in the presence of triethylamine (TEA) as the base, and using acetonitrile (MeCN) or Dimethylformamide (DMF) as solvent (**Scheme 2** and **Scheme 3**). Different reaction conditions were tested (TEA equivs, perfluoroarylated equivs, and reaction time) to optimize the synthetic methodology.
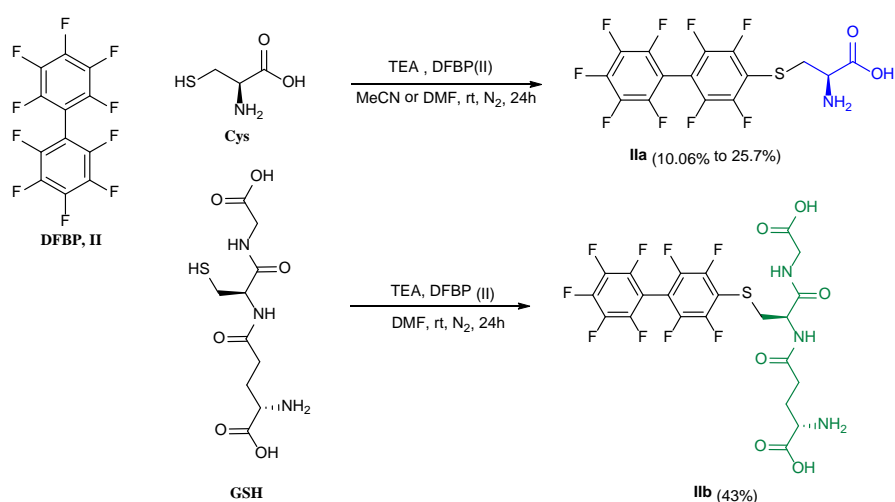
S-(perfluorophenyl)-L-Glutathione (C_6F_5-S-GSH, **Ib**) were also obtained at a meager yield of 5%, no matter the conditions used (**Scheme 2**). Like **Ia**, increasing the TEA or HFB equivs does not improve the reaction efficiency.
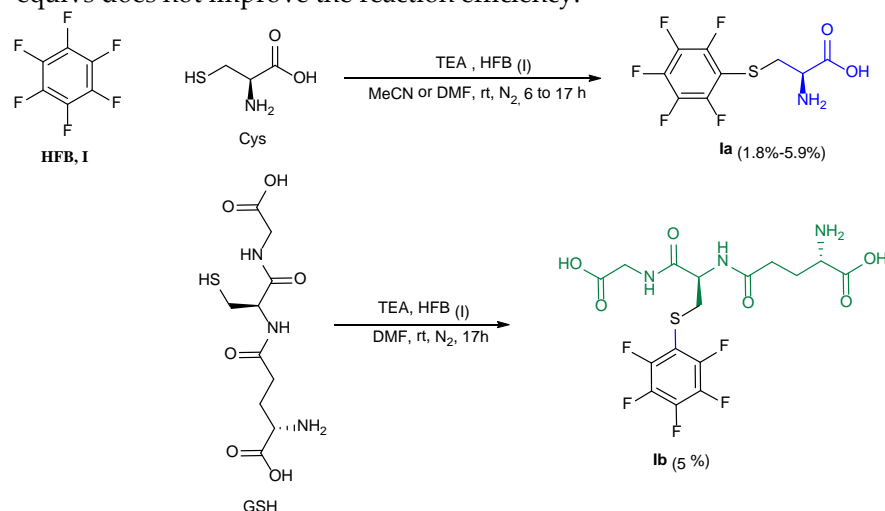
Scheme 2. Reaction conditions for the preparation of S-(perfluorophenyl)-L-cysteine (C_6F_5-S-Cys, **Ia**) and S-(perfluorophenyl)-L-Glutathione (C_6F_5-S-GSH, **Ib**).

C_6F_5-S-Cysteine (**Ia**) was isolated as a white solid at low yields of 1.8%, 5% and 5.9%, when 5, 8 and 10 equivalents of HFB (**I**) were used, respectively (**Scheme 2**).

A similar methodology was used to obtain S-(perfluoro-[1, 1'-biphenyl]-4-yl)-L-cysteine ($C_{12}F_9$-S-Cys, **IIa**) and S-(perfluoro-[1, 1'-biphenyl]-4-yl)-L-glutathione ($C_{12}F_9$-S-GSH, **IIb**) (**Scheme 3**). The equivalents of the TEA, the DFBP (**II**), and the solvent were modified, searching for better reaction conditions.

Scheme 3. Reaction conditions for the preparation of S-(perfluoro-[1,1'-biphenyl]-4-yl)-L-cysteine ($C_{12}F_9$-S-Cys, **IIa**) and S-(perfluoro-[1,1'-biphenyl]-4-yl)-L-glutathione ($C_{12}F_9$-S-GSH, **IIb**).

DFBP modifying cysteine ($C_{12}F_9$-S-Cys, **IIa**) was obtained as a white solid with 10.06% to 25.7% yield when TEA equivalents were increased from 5 to 7.5. DFBP (**II**, 10 equivs) was also successfully bounden to reduced glutathione (GSH, 1 equiv) using DMF as a solvent with a moderate yield of 43 %.

In general, the better results for the mono-S-alkylation reaction of perfluorinated compounds **Ia-b** and **IIa-b** were those in which a higher excess (10 equivs) of HFB (**I**) and DFBP (**II**), 5 equivs of TEA, and 24 hours of reaction were applied.

The reactions were followed by RP-HPLC and RP-HPLC-ESI, showing a control reaction time for **Ia-b** tighter than **IIa-b** due to the rapid formation of the S-substituted 1,4-tetrafluorobenzenes. The reduced glutathione (GSH)-base perfluorinated derivatives **Ib** and **IIb** were purified by RP column chromatography to obtain high-purity final products (See Experimental Section and Supporting Information).

Knowing that the mono addition using decafluorobiphenyl (DFBP, **II**) was more effective than with hexafluorobenzene (HFB, **I**), we carried out the perfluoroaryl mono addition of more complex Cys containing peptide using the perfluorobiphenyl scaffold (**II**) (**Scheme 4**). For that purpose, rodhamine B(RHB)-Cys containing peptide with 29 amino acid residues was synthetized by SPPS (See experimental section and Supporting Information); and then, using the optimized reaction conditions for **IIb**, and after a RP-column chromatographic separation, the perfluoarylated peptide **IIc** was yielded in 36% and 90.4% of purity.
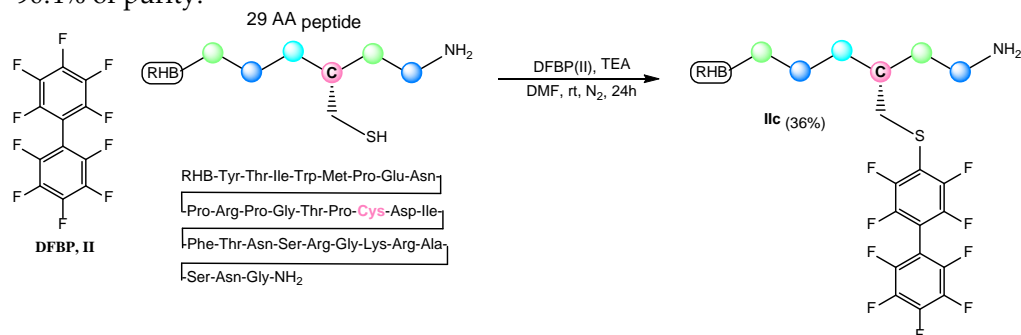
**Scheme 4**. RHB-Cys-containing peptide perfluoroarylation with DFBP (**IIc**).

Monoalkylated HFB and DFBPderivatives **Ia-b** and **IIa-b** were characterized by Infrared spectroscopic, ^{19}F-Nuclear Magnetic Resonance, and mass spectrometry, corroborating the proposed structures (See Experimental Section and Supporting Information).

IR spectra analysis confirmed the most representative functional groups in synthesized structures, showing characteristic peaks, especially those that demonstrate cysteine and reduced glutathione appendage for **Ia-b** and **IIa-b**, respectively. In general, a broadband ~3350 cm⁻¹corresponding to –OH stretching is observed. Furthermore, peaks at ~2900 cm⁻¹ are highlighted as belonging to C-H (sp³) stretching. Additionally, the C=O stretch signal corresponding to the carboxylic acid is observed at ~1700 cm⁻¹. Two bands at ~1650 and 1570 cm⁻¹ are assigned to the N-H bending, asymmetric and symmetric, respectively, of primary amine. Moreover, peaks corresponding to C=C stretch vibrations to the aromatic ring, which are often observed in pairs at 1600 cm⁻¹ and 1475 cm⁻¹, for characterized structures appear at 1416 cm⁻¹ and 1375.63 cm⁻¹; the observed deviation is due to the presence of the Fluor atoms in the aromatic ring. In addition, multiple peaks at the fingerprint region (1260.32 cm⁻¹ -1025.03 cm⁻¹) belong to the numerous C-F stretching. According to the previous report, all described signals appear at expected IR spectrum regions 20].

¹⁹F-Nuclear Magnetic Resonance is especially useful when polyfluorinated derivatives are obtained. When a modification happens in the highly symmetric HFB (**I**) or DFBP (**II**), the ¹⁹F-NMR spectrum goes from one signal corresponding to all equivalent fluorines to multiple signals, corroborating the structural transformation.

2.1.2. Bioconjugation as proof of concept for potential application of perfluoroarylated derivatives

 With the monosubstituted perfluoroarylated thiol-reactive compounds in hand (**Ib**, **IIb** and **IIc**), two different ways of bioconjugation through the thiol groups present in the antibody Anti-CD4 were tackled (**Scheme 5**). First, the conjugation was performed through the post translational modification of the carboxylic acids presents into Anti-CD4 by an amide bond formation with a cystamine, which, previous reduced procedure with DTT, allows to obtain the thiols (–SH) functionalized mAb (**Scheme 5**, Strategy 1).
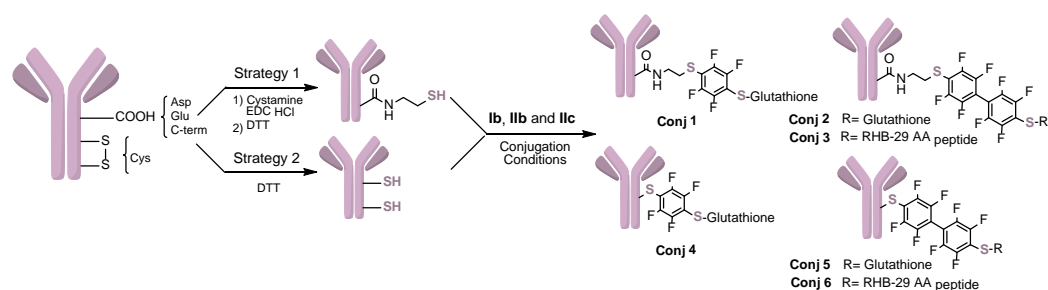
Scheme 5. Conjugation strategies.

The other way consisted of disulfide bond reduction from the antibody to generate the sulfhydryl groups available for bioconjugation (**Scheme 5**, Strategy 2). The bioconjugation was carried out using the modified mAb´s obtained in both strategies and the perfluorinated compounds previously synthesized (**Ib**, **IIb** and **IIc**) to furnish the corresponding conjugates. After separating any unconjugated linker-cargo (See experimental section), the purified ADCs were analyzed by reducing SDS-PAGE and mass spectrometry (See Experimental Section and Supporting Information).

The analysis by reducing SDS-PAGE of conjugates (See Supporting Information) showed that the conjugation strategies used with the antibody took place homogeneously. Moreover, the light and heavy chain integrity were maintained after the bioconjugation. The low molecular weight of the conjugated molecules hampers qualitative mass analysis by electrophoresis due to the slight difference between the naked and conjugated antibodies.

The intact conjugate mass analysis corroborated the integrity of the conjugate (**Figure 1**, conjugates 1 (B), 2 (C) and 4 (D)) (See Experimental section and Supporting Information).
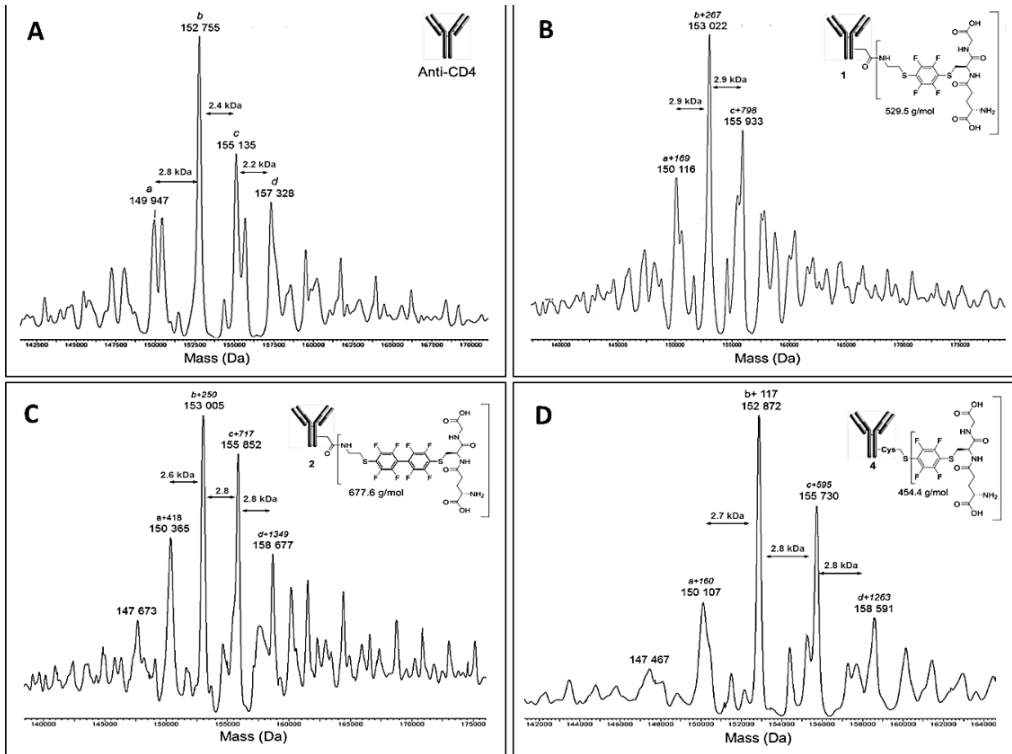
Figure 1. A,B,C,D correspond to Anti-CD4, Conjugates 1, 2 and 4 mass analysis (TOF ES$^+$), respectively.

2.1.3. Antibody-Conjugate cell binding analysis.

To determine whether the conjugation of the linkers to the anti-CD4 HP2/6 mAb has any effect on the binding to its CD4 epitope, we performed an antibody binding analysis on Jurkat T cells that naturally express CD4 on the cell surface. We used different concentrations (0.1-10 µg/ml) of the naked anti-CD4 HP2/6 mAb and the conjugates 1-6 (**Figure 2** and **Table 1**).
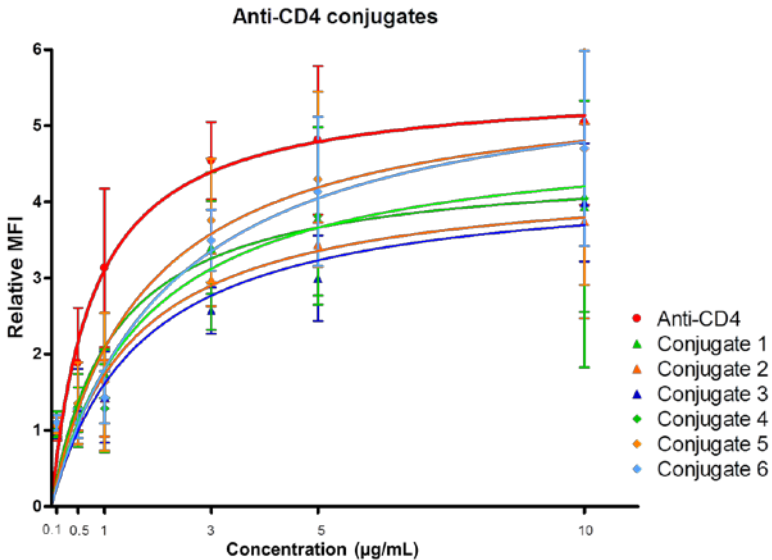
Figure 2. Analysis of the binding of anti-CD4 HP2/6 mAbs and the different conjugates to Jurkat T cells by flow cytometry. Jurkat T cells were incubated with the indicated concentrations of anti-CD4 mAb and the conjugates 1-6 followed by incubation with FITC-labelled goat anti-mouse IgG antibodies as described in Materials and Methods. Cytometry analysis was performed, and the mean fluorescence intensity (MFI) ratio was calculated using as a reference the MFI value or an irrelevant mAb (basal MFI value).

Table 11. Conjugate affinity is indicated as the conjugate concentration required to obtain half of the maximum mean fluorescence intensity (AC50) and the percentage of binding relative to that of the natural anti-CD4 mAb.

	AC_{50} (µg/ml)	max MFI %
Anti-CD4 mAb	0.95	100
Conjugate 1	1.65	73
Conjugate 2	2.20	62
Conjugate 3	2.65	74
Conjugate 4	2.55	75
Conjugate 5	2.02	91
Conjugate 6	2.37	91

2.2 Theoretical approach to monosubstituted-perfluoroaromatic derivatives

Theoretical calculations were applied to delve into spectroscopic characteristics and to explore the potential bioactivity of perfluorinated derivatives **Ia-b** and **IIa-b**. The results open the possibility of having tools to characterize similar derivatives in the future. In this sense, FT-IR and ^{19}F-NMR spectra were simulated and compared with those previously obtained.

2.2.1   Infrared Spectroscopy Simulation

Simulated FT-IR spectra of **Ia-b**, and **IIa-b** molecules were obtained using computational methods and compared to the experimental ones (**Table 2** and **Figure 3**). The vibrational spectral analysis of these compounds was done based on the characteristic vibrations of their methylene, carbonyl, aromatic, O-H, and N-H groups. The correlation graph between experimental and theoretical wavenumbers showed an excellent agreement between experimental and calculated values with a correlation (R^2) value of 0.9995 (**Figure 4**).

Table 2. FT-IR wavenumbers, experimental assignments, and DFT simulated wavenumbers with probable assignments and vibrational mode automatic relevance determination (VMARD) of **Ia**.

N°	Experimental FT-IR		Theoretical wavenumber (cm^{-1})		Vibrational assignment with VMARD ≥10%	
	Wavenumber (cm^{-1})	Intensity	Unscaled	Scaled	Description	Percent
1			434.00	433,39	υ C(14)-C(18)	11.1%
2	450,33	96,108	448.43	447,80	δ C(8)-C(11)-C(12)	10.0%
3	539,79	96,463	538.71	537,96	δ C(14)-C(18)-O(23)	12.3%
4			587.51	586,69	δ C(7)-C(9)-C(10)	12.4%
5			654.89	653,97	τ F(4)-C(11)-C(8)-C(7)	10.1%
6			672.80	671,86	τ F(6)-C(7)-C(8)-C(11)	19.6%
7			681.59	680,64	υ S(5)-C(13)	12.6%
8	723,38	95,777	736.04	735,01	τ C(9)-C(7)-C(8)-C(11)	18.1%
9	802,27	86,908	854.85	853,65	υ C(14)-N(19)	10.9%
10			945.00	943,68	τ O(23)-C(18)-O(20)-H(24)	16.3%
11			999.36	997,96	υ F(3)-C(10)	11.4%
12			1009.63	1008,22	υ C(13)-C(14)	10.6%
13	1024,73	84,584				
14			1109.28	1107,73	υ F(6)-C(7)	18.6%
15	1094,78	82,282	1118.83	1117,26	υ C(14)-N(19)	20.5%
16			1151.05	1149,44	υ C(14)-N(19)	10.7%

|						
17	1165,35	90,458	1166.34	1164,71	υ F(2)-C(9)	16.2%
18			1221.76	1220,05	υ C(18)-O(20)	35.0%
19			1250.13	1248,38	υ C(8)-C(11)	15.0%
20	1260,46	84,190	1270.63	1268,85	δH(17)-C(14)-C(18)	12.2%
21	1297,86	93,611	1312.35	1310,51	υ F(1)-C(8)	11.9%
22			1334.48	1332,61	δH(17)-C(14)-C(18)	11.1%
23	1376,21	86,654				
24	1403,34	92,336	1401.65	1399,69	δH(17)-C(14)-N(19)	11.7%
25	1411,33	92,377	1411.54	1409,56	υ C(10)-C(12)	14.6%
26	1461,28	73,765	1455.11	1453,07	δC(18)-O(20)-H(24)	29.2%
27			1489.85	1487,76	δH(15)-C(13)-H(16)	31.0%
28			1498.83	1496,73	υ F(4)-C(11)	10.4%
29	1540,75	96,387	1521.19	1519,06	υ F(6)-C(7)	15.1%
30	1601,13	93,235	1611.78	1609,52	υ C(7)-C(9)	17.3%
31	1620,96	92,326	1624.04	1621,77	υC(9)-C(10)	19.9%
32	1645,52	92,658				
33	1652,23	92,622	1680.74	1678,39	δH(21)-N(19)-H(22)	43.9%
34	1739,17	86,872	1821.04	1818,49	υ C(18)-O(23)	70.4%
35	2727,48	97,311				
36	2851,46	41,304				
37	2921,30	9,843	2950.72	2946,59	υ C(14)-H(17)	84.8%
38	2953,76	50,421	2993.99	2989,80	υ C(13)-H(16)	53.0%
39	3028,68	97,228	3049.38	3045,11	υ C(13)-H(15)	56.4%
40	3260,80	94,584	3276.81	3272,22	υ O(20)-H(24)	62.0%
41	3439,25	92,733	3442.30	3437,48	υ N(19)-H(21)	51.7%
42	3501,70	94,323	3509.64	3504,73	υ N(19)-H(22)	57.1%
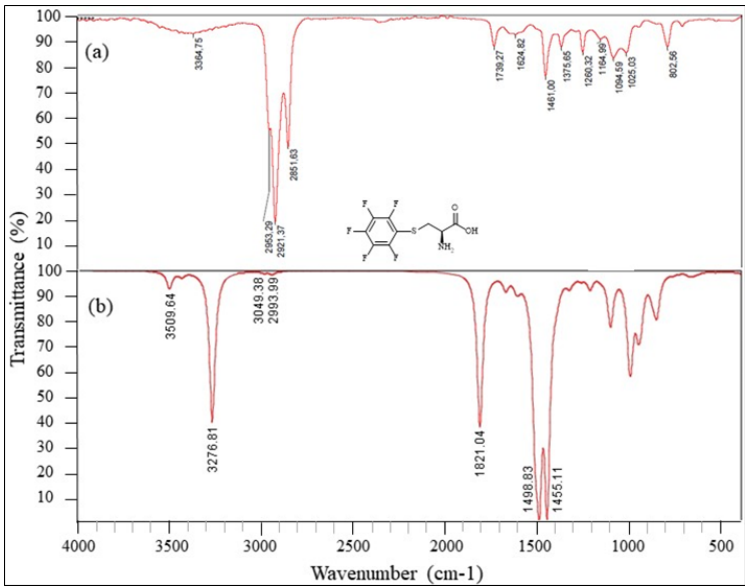
Figure 3. IR spectra of S-(perfluorophenyl)-L-cysteine (**Ia**): (**a**) experimental and (**b**) calculated.
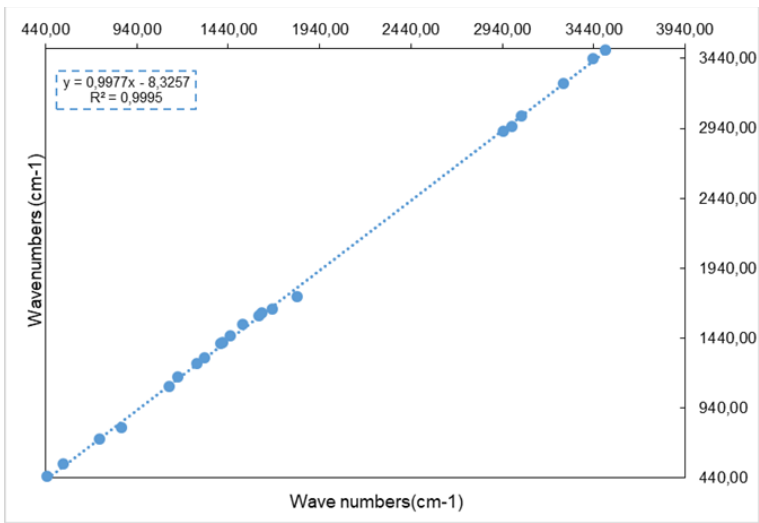
Figure 4. Correlation between the experimental and DFT vibrations of S-(perfluorophenyl)-L-cysteine (**Ia**).

2.2.2 ^{19}F-NMR spectroscopy simulation

Simulated 19F-NMR shift data for the hexafluorobenzene and decafluorobiphenyl derivatives (**Ia-b** and **IIa-b**) were calculated and compared to the experimental ones (**Table 3** and **Table 4**). Calculated chemical shifts give an error range between 1.46 -9.58 ppm concerning the experimental ones. Although the error reached nearly 9.60 ppm for hexafluorobenzene, the R^2 coefficient of the correlation between the calculated and experimental values was significantly higher for its derivatives 0.9926 and 0.9961 for **Ia** and **Ib**, respectively (**Figure 5a**). In the case of decafluorobiphenyl derivatives (**IIa-b**), error values are lower, and the R^2 coefficient larger than 0.9698 (**Figure 5b**).

Table 3. Calculated and experimental ^{19}F-NMR chemical shifts for hexafluorobenzene derivatives (**Ia-b**)
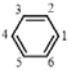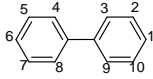
Resonance	I			Ia			Ib		
	Calcu-	Observed	Δ	Calcu-	Observed	Δ	Calcu-	Ob-	Δ
F-1	-155.32	-164.9	9	—	—		—	—	
F-2	-155.27	-164.9	9	-126.71	-132.16	5.4	-125.19	-133.09	7.9
F-3	-155.12	-164.9	9	-156,51	-161.74	5.2	-157,63	-161.68	4.0
F-4	-155.14	-164.9	9	-145,68	-149.74	4.0	-145,39	-153.04	7.6
F-5	-155.29	-164.9	9	-155,26	-161.74	6.4	-155,96	-161.68	5.7
F-6	-155.32	-164.9	9	-124,40	-132.16	7.7	-124,47	-133.09	8.6

Table 4. Calculated and experimental 19F NMR chemical shifts for hexafluorobenzene derivatives.

Resonance	II			IIa			IIb		
	Cal-	Ob-	Δ	Calcu-	Ob-	Δ	Calcu-	Ob-	Δ
F-1	-	-150.16	5.4						
F-2	-	-160.75	3.6	-123,96	-131.72	7.7	-129,57	-133.15	3.5
F-3	-	-137.69	8.3	-129,93	-136.27	6.3	-131,99	-133.47	1.4
F-4	-	-137.69	8.3	-129,52	-137.18	7.6	-129,95	-133.91	3.9
F-5	-	-160.75	3.6	-158,72	-160.23	1.5	-158,83	-161.73	2.9
F-6	-	-150.16	5.4	-145,10	-149.46	4.3	-146,31	-153.04	6.7
F-7	-	-160.75	3.6	-158,77	-160.23	1.4	-159,13	-161.73	2.6
F-8	-	-137.69	8.3	-129,77	-137.18	7.4	-130,39	-133.91	3.5

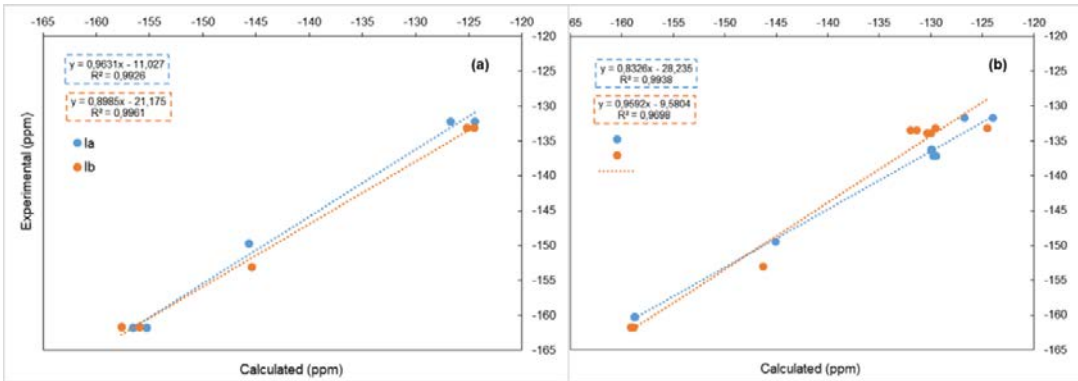|									
F-9	-	-137.69	8.3	-129,90	-136.27	6.3	-131,36	-133.47	2.1
F-10	-	-160.75	3.6	-126,73	-131.72	4.9	-124,50	-133.15	8.6

Figure 5. Correlation between the experimental and DFT calculated shifts. (**a**) Hexafluorobenzene derivatives **Ia-b** and (**b**) decafluorobiphenyl derivatives **IIa-b**.

2.2.3   A theoretical approach to the biological activity

Liker-cargoes' biological activity was tested through a DFT study and molecular Docking, for antimicrobial and anti-inflammatory activity. Calculated chemical reactivity parameters of liker-cargoes are shown in **Table 5**.

Table 5. Quantum chemical reactivity parameters HFB and DFBP derivatives (**Ia-b** and **IIa-b**).

Com-pounds	E_{HUMO}	E_{LUMO}	Energy Gap	σ	μ	χ	η	ω
			(eV)	(eV^{-1})			(eV)	
Ia	-6.648	-1.227	-5.421	0.368	-3.938	3.93	2.71	2.85
Ib	-6.626	-1.314	-5.312	0.377	-3.970	3.97	2.65	2.96
IIa	-6.834	-1.923	-4.911	0.407	-4.379	4.37	2.45	3.90
IIb	-6.529	-1.779	-4.750	0.421	-4.154	4.15	2.37	3.63

-Docking studies on perfluorated derivatives **Ia-b** and **IIa-b** for anticancer activity targeting DNA topoisomerase IIα.

DNA topoisomerase IIα is the molecular target of doxorubicin, an active drug used in breast cancer therapy. Molecular Docking on perfluorinated derivatives **Ia-b** and **IIa-b** against Human DNA Topoisomerase II α (PDB ID 3QX3) was carried out, and the affinity and residual amino acid interactions were established (**Table 6**).

Table 6. Results of Molecular Docking against Human DNA Topoisomerase II α (PDB ID 3QX3)

Ligands	Affinity (Kcal/mol)	DNA	Residual Amino acid interactions		LA involved in polar interactions
			Polar interactions /H-	No-polar interac-	
Ia	-6.7	DG-13, DA-	—	Asp-479, Arg-503	O(19)-H(23),
Ib	-8.1	DA-12, DT-9. DG-10	Lys-456, Asp-479	Arg-503, Gln-778	O(4)
IIa	-9.5	DG-13, DA-12, DT-9	Asp-479, Ser-480, Ala-481.	Asp-557, Glu-477, Arg-503	O(22), O(29)-H(33)
IIb	-10.0	DT-9, DG-13, DA-12, DC-11, DG-10.	Arg-820, Ser-818, Arg-820, Ala-817	Gln-778, Arg-503, Met-782.	O(6), O(2), O(3)-H(34)

*LA: ligand atoms

-Docking studies on perfluorinated derivatives **Ia-b** and **IIa-b** for anti-inflammatory activity targeting Cyclooxygenase-2 (COX-2).

Cyclooxygenase-2 (COX-2) is an enzyme responsible for the production of prostaglandins, lipid molecules related to pain and inflammation. Molecular Docking on perfluorinated derivatives **Ia-b** and **IIa-b** against Human DNA Topoisomerase II α (PDB ID 3QX3) was carried out, and the affinity and residual amino acid interactions were established (**Table 7**).

Table 7. Results of Molecular Docking against Human Cyclooxygenase-2 (PDB ID: 5F19)

Ligands	Affinity (Kcal/mol)	Residual Amino acid interactions		LA involved in polar interactions
		Polar interactions /H-bond	No-polar interaction	
Ia	-7.2	Arg-44, Asp-125, Ala-151, Arg-469	Cys-41, His-38, Asn-43, Gly-45, Val-46, Leu-123, Thr-129, Tyr-130, Arg-149, Leu-152, Pro-153, Gln-461, Gly-465.	O(22), O(19)-H(23), N(18)-H(21), N(18)-H(20)
Ib	-9.4	His-38, Arg-44, Cys-47, Ala-151, Pro-154, Gln-461	Cys-36, Pro-40, Cys-41, Gln-42, Asn-43, Gly-45, Val-46, Asp-125, Leu-152, Pro-153, Glu-465, Lys-468, Arg-469.	O(1), N(8)-H(29), O(4), O(3)-H(34), O(2), O(5)-H(36), O(6)
IIa	-9.4	——	Asn-34, Cys-36, Cys-37, Ser-38, His-39, Pro-40, Cys-41, Gln-42, Gly-45, Val-46, Cys-47, Met-48, Ser-49, Tyr-130, Gly-135, Tyr-136, Leu-152, Pro-153, Pro-154, Val-155, Pro-156, Gln-461, Glu-465, Tyr-466, Arg-469.	——
IIb	-10.8	Cys-41, Asn-43, Arg-44, Gly-45, Asp-125, Lys-468, Arg-469.	Asn-34, Cys-36, Cys-37, His-39, Pro-40, Gln-42, Val-46, Cys-47, Met-48, Ser-49, Thr-129, Tyr-130, Gly-135, Tyr-136, Lys-137, Ala-151, Leu-152, Pro-153, Pro-154, Val-155, Pro-156, Gln-461, Glu-465.	O(2), O(6), O(5)-H(36), N(7)-H(26), O(4), O(3)-H(34), N(8)-H(30).

3. Discussion

Five monoalkylated-perfluoarylated derivatives, **Ia-b** from HFB (**I**) and **IIa-c** from DFPB (**II**), were prepared using different reaction conditions (**Schemes 2-4**). Related to **Ia-b**, all conditions tested allowed to obtain the expected products S-(perfluorophenyl)-L-cysteine (C₆F₅-S-Cysteine, **Ia**), and S-(perfluorophenyl)-L-Glutathione (C₆F₅-S-GSH, **Ib**) with low yields (**Scheme 2**). The results showed that an increase in the base equivalents from 5 to 7 eq did not improve the yield. A change of solvent from acetonitrile to dimethylformamide did not contribute significantly to the efficiency of this reaction. The slight yield increase using DMF as the solvent could be due to the enhancement of the solubility of the reagents, favoring the homogeneity of the reaction.

Despite the low yields, it is also important to note that rigorous control of the reaction conditions was needed to obtain the mono-alkylated products (**Ia-b**). These perfluoroarylated compounds showed a high tendency to suffer double (1,4) aromatic nucleophilic substitution in front of a Cys-thiol group[15,21], explaining the low yields. The double alkylation at positions 1, and 4 of the aromatic ring is favored by (1) the steric hindrance

at the ortho position and (2) the activation of the para position due to the formation of the thioether group in the aromatic ring. Otherwise, it will lead to the 1,4-dialkyalted perfluoro aromatic rings, generating unreacted S-disubstituted perfluoroaryl derivatives, losing the potential site for a second functionalization, and lacking interest for potential applications. Despite strict control of reaction conditions, the dialkylated perfluorinated derivatives were the main by-product during the mono-adduct preparation, and HPLC and ^{19}F-NMR techniques confirmed its presence (See Supporting Information).

Monoalkylated DFBP derivatives **IIa-c** were obtained with moderate yields from 26 to 43%. In these cases, solvent plays a key role in the reaction efficiency; it even could be a cause that the reaction did not work when MeCN was employed as the solvent, as it was predictable because of the reaction mechanism. The reaction between a sulfhydryl and a perfluorinated molecule follows the $S_N Ar$ pattern. Specifically, through an addition-elimination mechanism comprising the formation of the Meisenheimer complex as the intermediate, hence solvation effects in this intermediate must influence the reaction success[22,23]. Similar results were reported by Alapour et al. [24] when employing *N*,*N*-dimethylformamide (DMF), *N*-methylpyrrolidone (NMP), dichloromethane (DCM) and toluene in a $S_N Ar$ with DFBP (**II**).

All monoalkylated perfluorinated derivatives **Ia-b** and **IIa-c** were characterized through spectroscopic techniques, unambiguously corroborating the proposed structures.

Two strategies for reduced glutathione (GSH)-based perfluoro-mono-alkylated derivatives (**Ib**, and **IIb**), and RHB-Cys-based perfluoro-mono-alkylated derivative (**IIc**) and Anti-CD4 bioconjugation were carried out through the thiol groups present in the antibody to assess a potential application of these kinds of products.

Conjugates mass analysis corroborated the integrity of prepared conjugates (**Figure 1** and Supporting Information). Despite detecting a broad isotopic envelope hindering the proper investigation of the bioconjugates, the major mass increment was observed with conjugates **1**, **2** and **4** where all the peaks suffer an increment which is possible to attribute to the cysteamine or the perfluorinated linker incorporation. In this sense, compared with peak c from the naked antibody in the analysis for the mentioned conjugates, a mass increment of 798, 717 and 595 Da for conjugates **1**, **2** and **4,** respectively, have been shown. This peak increase could correspond to the attachment of one molecule of the compounds **Ib** or **IIb**. It is important to consider that strategy 1 (**Conjugates 1-3**) introduce into the antibody one cystamine or in other words, two cysteamine residues (154 Da) once the cystamine is reduced. Furthermore, a higher difference with peak d from **Figure 1**A is assessed in **Figure 1**C (1349 Da) and D (1263), indicating the possibility that at least two molecules were attached to the antibody. On the contrary, the incorporation of the 29-amino acid residues peptide (**IIb**) is not detected by mass spectrometry for both tested strategies (see experimental section and Supporting Information).

Related to the cell binding analysis of conjugates (**Figure 2** and **Table 1**), the naked anti-CD4 HP2/8 mAb shows a higher mean fluorescence intensity and a higher binding affinity (AC_{50} = 0.95 µg/ml, indicated as the antibody concentration (AC)) needed to achieve 50% of the higher MFI value for each conjugate). Conjugates 5 and 6 have reduced binding affinity compared to the anti-CD4 mAb (AC_{50} 2 µg/ml and 2.37 µg/ml, respectively), although they reach a similar maximum mean fluorescence intensity value (91 % in both cases) than the anti-CD4 mAb (**Table 1**). This result suggests that conjugates **5** and **6** coat all available CD4 molecules on the cell surface. Conjugates **1**, **2**, **3** and **4** had AC_{50} of 1.65, 2.2, 2.65, and 2.55 µg/ml, respectively, but only returned 62-75% of the maximum MIF obtained using the naked anti-CD4 mAb. However, this reduction in the maximum MFI obtained with these conjugates might reflect a diminished binding of the secondary FITC antibody due to epitope masking caused by the linkers. The synthesized conjugates maintain their binding ability to CD4, similar to the naked antibody. This result indicates that both conjugation strategies tested did not disrupt the antibody activity, making perfluoroarylated compounds suitable linkers for ADCs.

Theoretical calculations were used to simulate IR and ^{19}F-NMR spectra to perfluoro-monoalkylated derivatives **Ia-b** and **IIa-b**. For all of them, it was appreciated that the accuracy of computed harmonic vibrational values is comparable with the experimental ones for a wide region of vibrational frequencies. Related to IR analysis, calculated and experimental vibrations of functional groups such as N-H, O-H, C-H (sp^3), C=O, and C=C (aromatic) are at very similar wavenumbers. Although FT-IR stretching mode of C-S bond usually appears at 696- 685 cm-1[25], experimentally, this vibration is not observed, but it agrees with the calculated one at 680,64 cm^{-1}. Based on these results, it is possible to conclude that the computational method is good enough to simulate IR spectra for perfluoro-aromatics derivatives.

Regarding ^{19}F-NMR simulations, the high correlations between experimental and simulated results indicate that the computational ^{19}F-NMR method is accurate[26,27], hence could be used for peak assignments and unambiguously determine the structure of hexafluorobenzene and decafluorobiphenyl derivatives. Thus, in this work, simulated chemical shifts help to confirm the assignment done in the experimental ^{19}F NMR spectra.

The calculated chemical reactivity parameters of liker-cargoes **Ia-b** and **IIa-b** were also analyzed (**Table 5**). The energy gap, which is the difference between HOMO and LUMO, showed that all derivatives Ia-b and IIa-b are stables. However, HFB derivatives (**Ia-b**) have a higher energy gap value indicating that DFBPs derivatives (**IIa-b**) have a greater capacity to transfer charge density from HOMO to LUMO, that is, **IIa-b** is softer than **Ia-b**. Additionally, a large energy gap increases the global hardness of compounds as follows: **Ia>Ib>IIa>IIb**, and their chemical reactivity decrease in the reverse order: **Ia<Ib<IIa<IIb** [28]. These results show that all compounds exhibit a low energy gap, suggesting a significant intramolecular charge from HOMO to LUMO groups and high chemical reactivity[29,30]. Besides, like electronegativity and hardness, the electrophilicity index ω, as an indicator of reactivity, measures the stabilization energy when the system acquires an additional electronic charge [31]. It can be seen how ω is higher for the DFBP derivatives (**IIa-b**), evidencing the greater tendency of the HFB derivatives (**Ia-b**) to accept electrons from the environment. Moreover, compounds **IIa** and **IIb** have larger global softness (σ, eV^{-1}), electronegativity (χ, eV), and global electrophilicity (ω, eV); therefore, they could have good bioactivity[32].

The Molecular Docking on perfluorinated derivatives **Ia-b** and **IIa-b** against Human DNA Topoisomerase II α (PDB ID 3QX3) indicates that compounds **Ib**, and **IIa-b** show a strong binding affinity towards the mentioned target (**Table 5**) with binding energy values ranging from -8.1 to -10.0 Kcal/mol compared to vosaroxin (−6.2 kcal/mol)[29]. S-(perfluoro-[1, 1'-biphenyl]-4-yl)-L-cysteine (**IIa**) and S-(perfluoro-[1, 1'-biphenyl]-4-yl)-L-glutathione (**IIb**) present the higher binding affinity -9.5 and 10.0 Kcal/mol. Both interact with Arg-503 amino acid residue and DT-9, DG-13, and DA-12 nucleic acid residues compared with vosaroxin. This result suggests that **IIa** and **IIb** could be potential topoisomerase II α inhibitors, becoming potential anticancer agents.

Molecular Docking on perfluorinated derivatives **Ia-b** and **IIa-b** against Human Cyclooxygenase-2 (COX-2) showed a robust binding affinity to **Ib**, and **IIa-b** (**Table 6**), with binding energy values ranging from -9.4 to -10.8 Kcal/mol compared to quercetin (−9.1 kcal/mol) which has a potent anti-inflammatory activity[33–35]. These three compounds interact via key amino acid residues such as Cys-41, Cys-47, Gln-461, and Glu-465, interacting with native ligand 2-acetamido-2-deoxy-beta-D-glucopyranose (NAG). These results indicate that compounds **Ib**, and **IIa-b** are selective COX-2 inhibitors [36]. Additionally, COX-2 protein has a large hydrophobic segment filled with Cys-36, Cys-47, and Met-48, which are reported to play a critical role as the ligand entry point to the active site of this enzyme[36]. Therefore, DFBP derivatives **IIa-b**, able to interact with Cys-36, Cys-37 and Met-48 could be better candidates for anti-inflammatory treatment.

4. Materials and Methods

3.1. Chemistry

3.1.1. General

All chemical reactions sensitive to moisture or air were carried out under a nitrogen atmosphere. All reagents employed were purchased from commercial suppliers and used without further purification. TLC was performed during the reactions using silica gel GF$_{254}$ precoated plates (0.20–0.25 mm thickness) with a fluorescent indicator. The visualization of TLC plates was accomplished using a typical TLC indicator solution (10 % sulfuric acid/ethanol solution) and UV light (254 nm). High-Performance Liquid Chromatography (HPLC) apparatus Ultimate 3000, equipped with reverse phase C-18 column for HPLC Hypersil GOLD TM (150 x 4.6 mm), an autosampler, a Thermo Scientific ™ quaternary pump, a column compartment, and a photodiode array detector (PAD) was used for follower the reactions and to the analysis of all samples. The measurements were developed at two different wavelengths (220 and 280 nm), but the absorbance at 220 nm was the wavelength that gave us better results for peak analysis. Fourier-transformed infrared spectroscopy attenuated total reflectance (FTIR-ATR) was carried out on hexafluorobenzene (HFB, **I**), decafluorobiphenyl (DFBP, **II**), and their derivatives with cysteine and glutathione using spectrophotometer Agilent Cary 630 FTIR in a range of 4000-400 cm-1 with 32 sample scans and 32 background scans. ^{19}F-Nuclear Magnetic Resonance spectroscopy (^{19}F-NMR) was carried out on all perfluoroaromatics compounds using the NMReady60 spectrometer with a resonance frequency of 60 MHz in a permanent magnet from Nanalysis Corp. The number of scans given for each sample is 128 scans, typically 0.06 sec per scan at room temperature.

3.1.2. Synthesis and Characterization

Different reaction conditions were tested to optimize the synthesis of HFB derivatives **Ia-b** (**Table 8**) and DFBP derivatives **IIa-b** (**Table 9**).

Synthesis of S-(perfluorophenyl)-L-cysteine (C$_6$F$_5$-S-Cys, **Ia**) and S-(perfluorophenyl)-Glutathione (C$_6$F$_5$-S-GSH, **Ib**): In general, L-cysteine (0.43 mmol, 1 eq) for **Ia** or reduced glutathione (GSH) (0.43 mmol, 1 eq) for **Ib**, and established equivalents of hexafluorobenzene (HFB, **I**), and TEA were added in 30 mL of dry solvent. The reaction was left to react over 17 hours at room temperature under N$_2$ atmosphere. Then, the solvent was removed under vacuum conditions, and the crude reaction was purified on a microscale column using EtOAc/Hexane/EtOH (5/3/2) solution. Then, the solvent was removed from the desired collected fractions, dissolved in water, and lyophilized, obtaining **Ia** or **Ib** as a white solid.

S-(perfluorophenyl)-L-cysteine (C$_6$F$_5$-S-Cys, **Ia**): RP-HPLC: [linear gradient H$_2$O/MeCN (100:0) to (40:60) over 8 min] t_R = 4.127 min at 220nm; ATR FT-IR ν (cm^{-1}): 3364, 2953, 2921, 2851, 1739, 1625, 1461, 1376, 1260, 1165, 1095, 1025 and 802; ^{19}F NMR (CHCl$_3$) δ (ppm) = -132.16, -149.74 & -161.74

S-(perfluorophenyl)-L-Glutathione (C$_6$F$_5$-S-GSH, **Ib**): the reaction crude was purified on a pre-packed Redisep Rf Gold C18 13 g column by using H$_2$O/MeCN from 100:0 to 0:100 over 40 min. The collected fractions corresponding to the desired product were lyophilized, Purity 97%. RP-HPLC: [linear gradient H$_2$O/MeCN (100:0) to (0:100) over 8 min] t_R = 4.693 min at 280nm; ATR FT-IR ν (cm-1): 3368, 3340, 2922, 2873, 1654, 1460, 1403, 1284, 1049, 1006; ^{19}F-NMR (CHCl$_3$) δ = -57.8 (t, J = 9.3 Hz, 3F), -87.7 (q, J = 9.3 Hz, 2F), -119.9 (t, J = 9.3 Hz, 2F), -129.4 (s, 2F).m/z calculated for C$_{16}$H$_{16}$F$_5$N$_3$O$_6$S = 473.4; found [M+H]+ = 474.1

Table 8. Reaction conditions tested to **Ia-b**.

Compound	HFB (I) (equiv)	TEA (equiv)	Solvent	Yield (%)
Ia	5	5	MeCN	1.8

	8	5	MeCN	5
	8	5	DMF	5.2
	10	7	DMF	5.9
Ib	8	5	MeCN	4.9
	8	5	DMF	4.7.
	10	7	DMF	5.0

Synthesis of S-(perfluoro-[1,1'-biphenyl]-4-yl)-L-cysteine ($C_{12}F_9$-S-Cys, **IIa**) and S-(perfluoro-[1,1'-biphenyl]-4-yl)-Glutathione ($C_{12}F_9$-S-GSH, **IIb**): In general, L-cysteine (0.075 mmol, 1 equiv) for **IIa** and reduced glutathione (0.075 mmol, 1 equiv) for **IIb**, and established equivalents of decafluorobiphenyl (DFBP, **II**), and TEA were added in 30 mL of dry solvent. The reaction was left to react over 24 h at room temperature under N_2 atmosphere. After that, the solvent was removed under vacuum, and the crude reaction was purified on a microscale column using EtOAc/Hexane/EtOH (5/3/2) solution. Then, the desired collected fractions were collected using TLC. Later, the solvent was removed from the collected fractions, dissolved in water, and lyophilized, obtaining **IIa** and **IIb** as a white solid.

S-(perfluoro-[1,1'-biphenyl]-4-yl)-L-cysteine ($C_{12}F_9$-S-Cys, **IIa**): RP-HPLC: [linear gradient H_2O/MeCN (100:0) to (40:60) over 8 min] t_R = 4.203 min at 220nm; ATR FT-IR ν (cm^{-1}): 2976, 2604, 2495, 1618, 1497, 1469, 1389, 1300, 1263, 1131, 1053, 1000, 966, and 725; ^{19}F NMR ($CHCl_3$) δ (ppm) =-133.09, -153.04 & -161.68.

S-(perfluoro-[1,1'-biphenyl]-4-yl)-Glutathione ($C_{12}F_9$-S-GSH, **IIb**): the reaction crude was purified on a pre-packed Redisep Rf Gold C18 13 g column by using H_2O/MeCN from 90:10 to 0:100 over 45 min. The collected fractions were lyophilized. RP-HPLC: [linear gradient H_2O/MeCN (100:0) to (40:60) over 8 min] tR = 5.367min at 220nm, Purity 99%; ATR FT-IR ν (cm-1): 3351, 2926, 2874, 1731, 1661, 1534, 1468, 1408, 1285, 1222, 1157, 1055, 1009, and 955; ^{19}F-NMR (H_2O) δ = -57.8 (t, J = 9.3 Hz, 3F), -87.7 (q, J = 9.3 Hz, 2F), -119.9 (t, J = 9.3 Hz, 2F), -129.4 (s, 2F). . *m/z* calculated for $C_{22}H_{16}F_9N_3O_6S$ = 621.43; found [M+H]$^+$ = 622.1.

Table 9. Reaction conditions tested to **IIa-b**.

Compound	DFBP (II) (equiv)	TEA (equiv)	Solvent	Yield (%)
IIa	5	5	MeCN	-
	5	5	DMF	10.06
	8	8	DMF	25.7
	10	8	DMF	24.8
IIb	5	5	DMF	43
	10	8	DMF	43

Synthesis of $C_{12}F_9$-S-[RHB-peptide] (**IIc**):

RGV peptide was synthesized through automatized SPPS and then manually conjugated to rhodamine B (RHB) (See Supporting Information)

Synthesis of RHB-Tyr-Thr-Ile-Trp-Met-Pro-Glu-Asn-Pro-Arg-Pro-Gly-Thr-Pro-Cys(**C$_{12}$F$_9$**)-Asp-Ile-Phe-Thr-Asn-Ser-Arg-Gly-Lys-Arg-Ala-Ser-Asn-Gly-NH$_2$ (**IIc**)
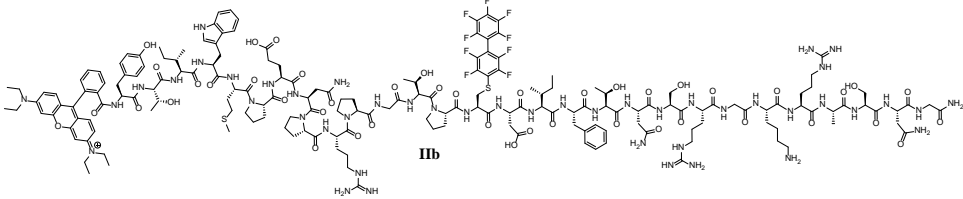
To a mixture of a thiol-free 29 amino acids peptide (RHB-YTIWMPENPRPG-TPCDIFTNSRGKRASNG-NH$_2$) (10 mg, 2.7 μmol) in 10 mL of dry DMF, decafluorobiphenyl (9 mg, 27 μmol) and TEA (0.4 μL, 5.5 μmol) were added, and then the reaction was stirred at room temperature under N_2 during 17 h. Afterward, the solvent was removed under vacuum, and the reaction crude was purified on a pre-packed Redisep Rf Gold C18

4.3 g column by using H_2O/MeCN from 100:0 to 0:100 over 15 min. The collected fractions were lyophilized, obtaining 3.9 mg (36%) of the monoalkylated product as a pale pink powder.

$C_{12}F_9$-S-RHB-Peptide (IIb): HPLC (H_2O/MeCN from 70:30 to 0:100 over 8 min): t_R: 4.5 min. m/z calculated for $C_{181}H_{246}F_9N_{46}O_{44}S_2+ = 4005.3$ Da; found $[M+5H]^{5+}/5 = 801.7$, $[M+4H]^{4+}/4 = 1002.0$ and $[M+3H]^{3+}/3 = 1335.6$.

Bioconjugation

Anti-CD4 characterization.

5 mL of Anti-CD4 (2 mg/mL) in saline solution antibody was dialyzed (MWCO: 12-14,000) over water and 5 mL of antibody over phosphate saline buffer (PBS). A sample of 1.20 mg/mL in water was diluted ¼ with 1% formic acid aqueous solution to 2.0 μM. Then 40 μL was injected for MS analysis.

General procedure

Strategy 1 (Conjugates 1-3)

A solution of Anti-CD4 in 0.1 M Na_3PO_4, 0.15 M NaCl at pH = 7.4 was treated with cysteamine dihydrochloride (20 eq) and EDC·HCl (>100 eq) for 2 h at room temperature. Afterward, the mixture was purified through PD-10 column, and the antibody-containing fractions were combined. Then the modified antibody was treated with DTT (>100 eq) for 30 min at room temperature. Then the solvent mixture was exchanged using a PD-10 column to a solution of 50 mM of Na_2HPO_4, 0.15 M NaCl and 10 mM of EDTA at pH = 7.2.

Then the cysteamine-modified antibody was left to react with the corresponding modified perfluoro compound (**Ib**, **IIb** and **IIc**), which was prepared following the above-described procedure. After that, the mixture was purified through PD-10 column or dialysis. Then the conjugates were analyzed by gel electrophoresis using 10% acrylamide under reducing conditions and by mass spectrometry.

Strategy 2 (Conjugates 4-6)

A solution of Anti-CD4 in 0.1 M Na_3PO_4, 0.15 M NaCl and 10 mM EDTA at pH = 7.2 was treated with DTT (3 eq) during 90 min at 37 ºC. Then the reduced antibody was purified using a PD-10 column, eluting with the same buffer solution. Then the reduced antibody was treated with the corresponding modified perfluoryl compound (**Ib**, **IIb** and **IIc**) which was prepared following the above described procedure. After that, the mixture was purified through PD-10 column or dialysis. Then the conjugates were analyzed by gel electrophoresis using 10% of acrylamide under reducing conditions and by mass spectrometry.

The specific procedure for each conjugate, SDS-Page, mass spectrometry and DAR results are included in the Supporting Information.

Binding affinity experiments:

Jurkat T cells (5×10^5) were incubated with the anti-CD4 HP2/6 mAb and with the anti-CD4 HP2/6 conjugates under study (conjugates 1-6) at the indicated concentrations and incubated on ice for 1 h. Then cells were washed twice with PBS (137 nM NaCl, 2.7 mM KCl, 10 mM Na_2HPO_4 and 1.8 mM KH_2PO_4) and incubated with 10 μg/ml of FITC-labelled anti-mouse IgG antibodies (BD biosciences) for 30 min on ice. The cells were washed twice in PBS and resuspended in PBS for their analysis by flow cytometry using a FACSCanto II (BD biosciences). **Table 10** shows the MFI ± SD for each conjugate and concentration tested. Results are expressed as the mean +/- SD of 3 independent experiments.

Table 10. Reaction conditions tested to **IIa-b**.

mAb (ug/mL)	Mean Fluorescence Intensity (MFI)± SD						
	Anti-CD4 mAb	Conj 1	Conj 2	Conj 3	Conj 4	Conj 5	Conj 6
0.1	1.02 ± 0.15	1.04 ± 0.07	0.99 ± 0.11	1 ± 0.11	1.08 ± 0.16	1.06 ± 0.1	1.1 ± 0.1
0.5	1.88 ± 0.73	1.35 ± 0.38	1.12 ± 0.12	1.29 ± 0.51	1.17 ± 0.39	1.35 ± 0.54	1.09 ± 0.19
1	3.13 ± 1.04	1.74 ± 0.32	1.42 ± 0.5	1.43 ± 0.59	1.29 ± 0.57	1.64 ± 0.9	1.3 ± 0.34

3	4.54 ± 0.51	3.34 ± 0.61	2.97 ± 0.34	2.57 ± 0.3	3.35 ± 1.03	3.76 ± 0.81	3.49 ± 0.4
5	4.81 ± 0.97	3.78 ± 1.01	3.44 ± 0.28	3 ± 0.56	3.81 ± 1.16	4.3 ± 1.14	4.14 ± 0.98
10	5.04 ± 1.08	3.94 ± 1.38	3.75 ± 1.27	3.99 ± 0.77	4.04 ± 2.21	4.69 ± 1.78	4.70 ± 1.28

3.2. Computational approach

3.2.1. Simulated IR spectra

All small molecules were built with Avogadro[37], and the structures were further optimized based on the MM2 force field. The orca inputs were generated using the same tool. Then, the structures were optimized using Density Functional Theory as implemented in Orca[38] and with gas phase. All compounds were optimized using B3LYP exchange-correlation functional and Def2-TZVP basis set. Molecules previously optimized were employed to calculate infrared (IR) frequencies. The calculated wavenumbers were ascended, employing 0.9986 as a uniform scaling factor to correct the overestimation from some negative factors, such as the incompleteness of the basis set and harmonic character[39]. Additionally, no implicit model of solvent, same basis set and functional were used, and IR spectrum was visualized in Gabedit[40]. Additionally, the distributions of calculated wavenumbers assignment were performed employing vibAnalysis software[41].

3.2.2. Simulated ^{19}F-NMR spectra

Molecules previously optimized were employed to calculate ^{19}F-NMR spectra using DFT method with a hybrid three-parameter B3LYP79 functional and DEF2-TZVPP106 basis set. Chloroform solvent was included as the CPCM implicit solvent model due to this was used for the experimental part. The computed isotropic shifts were scaled based on the equation $\delta = -0.99680\theta_{isotropic} + 184.92$, which is recommended for ^{19}F-NMR chemical shifts of fluorinated aromatic compounds [42].

3.2.3. Calculations related to the biological activity

Optimized structure coordinates of **Ia-b** and **IIa-b** were used to generate inputs for TDDFT calculation. The solvent in CPCM was DMF, maxdim was set as 5, and nroots (number of calculated transition states) was set to 50. The input was made based on RIJCOSX TDDFT calculation input as suggested by ORCA input library [43]. Throughout TDDFT calculation HOMO and LUMO values are obtained. Hence, global reactivity descriptor parameters were evaluated to ascertain the biological activity of perfluoroaryl derivatives. These parameters, such as electronegativity (χ), global hardness (η), global softness (S), chemical potential (μ), and global electrophilicity index (ω), were calculated as Abu-Melha reported [44].

3.3.4. Molecular Docking

The standard protocol of AutoDock Vina[45,46] was used to dock the proteins (PDB ID: 1T8I). Previously optimized chemical structures of compounds **Ia-b** and **IIa-b** were employed as linkers. The proteins' PDB structure was retrieved from RCSB Protein Data Bank, PDB (http://www.rcsb.org/). For each ligand, a maximum of nine conformers were determined throughout the docking process. The most favorable conformation (least binding energy) was chosen to analyze the interactions between the ligands and target receptors employing PyMOL.

Some fluoride compounds possess anticancer activity and act through the inhibition of nucleic acid synthesis[47–49]. Therefore, human topoisomerase II alpha (PDB ID: 3QX3) was used to test the bioactivity of synthesized linker cargoes. The protein preparation was

performed using the reported protocol[29,50], removing the crystallized ligand, cofactors, and water molecules. AutoDock graphical interface was employed to set the grid for molecular docking simulation whose lengths are 90, 90 and 90, pointing in x, y, and z directions for 3QX3. Additionally, the grid box for 6F86 is 60, 60 and 60. The grid spacing point was set to 0.375 Å, and the center grid box are (31.44 Å, 100.08 Å and 43.5 Å) and (61.46Å, 29.48Å and 61.69Å) for 3QX3 and 6F86, respectively.

Protein selection for anti-inflammatory activity was made according to the reported methodology by Maghfiroh, K. et al.[51]. The target was the PDB structure of Aspirin Acetylated Human Cyclooxygenase-2 (COX-2, PDB ID: 5F19). The protein preparation was performed using the reported protocol[51], removing the B sequence, crystallized ligand, cofactors, and water molecules. AutoDock graphical interface was employed to set the molecular docking simulation grid with lengths of 60, 60 and 60 pointing in x, y, and z directions, respectively. The grid spacing point was set to 0.375 Å, and the center grid box is (32.563 Å, 55.808 Å and 53.116 Å).

5. Conclusions

Cysteine-based perfluoroaromatic scaffolds (hexafluorobenzene (HFB, **I**) and decafluorobiphenyl (DFBP, **II**)) were synthesized via S_NAr reaction and established as a chemoselective and stable scaffold to simple or more complex systems. Decafluorobiphenyl (**II**) was more effective than hexafluorobenzene (**I**) for the monoalkylation of decorated thiol molecules.

The conjugation via the thiol group of antibodies (one of the most complex systems in nature) was studied using **I** and **II** moieties as non-cleavable linkers and the unique regioselectivity 1,4 of the S_NAr of these perfluoroaromatic rings. The two strategies of thiol-assisted conjugation were both effective, but the strategy that involves partial disulfide bond reduction of the antibody (Strategy 2) allowed better site-specific conjugation. Moreover, we demonstrated that this bioconjugation procedure preserved the binding activity to CD4 of these conjugates. Even though a reduction in the binding affinity of the conjugates to the antigen was observed, compared to the naked antibody, these conjugates maintain a high binding activity to the antigen, thus highlighting the suitability of the perfluoroarylation-based bioconjugation methods for the modification of bioactive antibodies.

Comparison of calculated and experimental ^{19}F-NMR shifts and IR wavenumbers give excellent correlations, indicating that ^{19}F-NMR and IR computations are powerful tools in structurally identifying HFB and DFBP derivatives. Thus, both methods could be employed to assign unknown perfluoroaromatics compounds.

Molecular Docking of synthesized compounds (**Ia-b**, **IIa-b**) against human topoisomerase II α, and human cyclooxygenase-2 (COX-2) revealed a promising scoring pose (lowest energy) with a value ranging from −8.1 to -10.0 Kcal/mol, and -9.4 to -10.8 Kcal/mol, compared to vosaroxin (−6.2 kcal/mol), and quercetin (−9.1 kcal/mol), respectively. S-(perfluoro-[1, 1′-biphenyl]-4-yl)-*L*-cysteine (**IIa**) and S-(perfluoro-[1, 1′-biphenyl]-4-yl)-*L*-glutathione (**IIb**) displayed comparable binding affinity (-9.5 and 10 kcal/mol) with vosaroxin (−6.2 kcal/mol), signifying they can be potential topoisomerase II α inhibitors and even might be used as anticancer agents. These compounds **IIa-b**, but also **Ib**, shows a high binding affinity to human cyclooxygenase-2 (-9.4, -9.4, and -10.8 kcal/mol) compared to quercetin (−9.1 kcal/mol). Therefore, they could be used as a potential anti-inflammatory agent. Finally, quantum chemical reactivity parameters suggested that HFB and DFBP derivatives are chemically reactive, showing the lowest gap energy.

Supplementary Materials: The following supporting information can be downloaded at: www.mdpi.com/xxx/s1, Figure S1: title; Table S1: title; Video S1: title.

Conflicts of Interest: The authors declare no conflict of interest.

References

1. Spicer, C.D.; Davis, B.G. Selective Chemical Protein Modification. *Nat Commun* **2014**, *5*, 4740, doi:10.1038/ncomms5740.

2. Greg T. Hermanson *Bioconjugate Techniques*; Elsevier, 2013; ISBN 9780123822390.

3. Smith, M.E.B.; Schumacher, F.F.; Ryan, C.P.; Tedaldi, L.M.; Papaioannou, D.; Waksman, G.; Caddick, S.; Baker, J.R. Protein Modification, Bioconjugation, and Disulfide Bridging Using Bromomaleimides. *J Am Chem Soc* **2010**, *132*, 1960–1965, doi:10.1021/ja908610s.

4. Baslé, E.; Joubert, N.; Pucheault, M. Protein Chemical Modification on Endogenous Amino Acids. *Chem Biol* **2010**, *17*, 213–227, doi:10.1016/j.chembiol.2010.02.008.

5. Schumacher, F.F.; Nobles, M.; Ryan, C.P.; Smith, M.E.B.; Tinker, A.; Caddick, S.; Baker, J.R. In Situ Maleimide Bridging of Disulfides and a New Approach. *Bioconjug Chem* **2011**, 132–136.

6. Yao, H.; Jiang, F.; Lu, A.; Zhang, G. Methods to Design and Synthesize Antibody-Drug Conjugates (ADCs). *Int J Mol Sci* **2016**, *17*, 194, doi:10.3390/ijms17020194.

7. Liu, P.; O'Mara, B.W.; Warrack, B.M.; Wu, W.; Huang, Y.; Zhang, Y.; Zhao, R.; Lin, M.; Ackerman, M.S.; Hocknell, P.K.; et al. A Tris (2-Carboxyethyl) Phosphine (TCEP) Related Cleavage on Cysteine-Containing Proteins. *J Am Soc Mass Spectrom* **2010**, *21*, 837–844, doi:10.1016/j.jasms.2010.01.016.

8. Junutula, J.R.; Raab, H.; Clark, S.; Bhakta, S.; Leipold, D.D.; Weir, S.; Chen, Y.; Simpson, M.; Tsai, S.P.; Dennis, M.S.; et al. Site-Specific Conjugation of a Cytotoxic Drug to an Antibody Improves the Therapeutic Index. *Nat Biotechnol* **2008**, *26*, 925–932, doi:10.1038/nbt.1480.

9. Shen, B.Q.; Xu, K.; Liu, L.; Raab, H.; Bhakta, S.; Kenrick, M.; Parsons-Reponte, K.L.; Tien, J.; Yu, S.F.; Mai, E.; et al. Conjugation Site Modulates the in Vivo Stability and Therapeutic Activity of Antibody-Drug Conjugates. *Nat Biotechnol* **2012**, *30*, 184–189, doi:10.1038/nbt.2108.

10. Chalker, J.M.; Bernardes, G.J.L.; Lin, Y.A.; Davis, B.G. Chemical Modification of Proteins at Cysteine: Opportunities in Chemistry and Biology. *Chem Asian J* **2009**, *4*, 630–640, doi:10.1002/asia.200800427.

11. Gunnoo, S.B.; Madder, A. Chemical Protein Modification through Cysteine. *ChemBioChem* **2016**, *17*, 529–553, doi:10.1002/cbic.201500667.

12. Stephens, R. Robson, Smith, Stephens, and Tatlow : 691. Aromatic Polyjuoro-Compound3. Part X1II.I Derivatives. **1962**.

13. Birchall, J.M.; Green, M.; Haszeldine, R.N.; Pitts, A.D. The Mechanism of the Nucleophilic Substitution Reactions of Polyfluoroarenes. *Chemical Communications (London)* **1967**, 338–339, doi:10.1039/C19670000338.

14. Li, J.; Deng, J.J.; Yin, Z.; Hu, Q.L.; Ge, Y.; Song, Z.; Zhang, Y.; Chan, A.S.C.; Li, H.; Xiong, X.F. Cleavable and Tunable Cysteine-Specific Arylation Modification with Aryl Thioethers. *Chem Sci* **2021**, *12*, 5209–5215, doi:10.1039/d0sc06576e.

15. Spokoyny, A.M.; Zou, Y.; Ling, J.J.; Yu, H.; Lin, Y.; Pentelute, B.L. A Perfluoroaryl-Cysteine SNAr Chemistry Approach to Unprotected Peptide Stapling. *J.a.C.S* **2013**, *135*, 5946–5949.

16.   Zou, Y.; Spokoyny, A.M.; Zhang, C.; Simon, M.D.; Yu, H.; Lin, Y.S.; Pentelute, B.L. Convergent Diversity-Oriented Side-Chain Macrocyclization Scan for Unprotected Polypeptides. *Org Biomol Chem* **2014**, *12*, 566–573, doi:10.1039/c3ob42168f.

17.   Zhang, C.; Welborn, M.; Zhu, T.; Yang, N.J.; Santos, M.S.; Van Voorhis, T.; Pentelute, B.L. π-Clamp-Mediated Cysteine Conjugation. *Nat Chem* **2016**, *8*, 120–128, doi:10.1038/nchem.2413.

18.   Alapour, S.; De La Torre, B.G.; Ramjugernath, D.; Koorbanally, N.A.; Albericio, F. Application of Decafluorobiphenyl (DFBP) Moiety as a Linker in Bioconjugation. *Bioconjug Chem* **2018**, *29*, 225–233, doi:10.1021/acs.bioconjchem.7b00800.

19.   Seo, M.; Shin, H.K.; Myung, Y.; Hwang, S.; No, K.T. Development of Natural Compound Molecular Fingerprint (NC-MFP) with the Dictionary of Natural Products (DNP) for Natural Product-Based Drug Development. *J Cheminform* **2020**, *12*, 1–17, doi:10.1186/s13321-020-0410-3.

20.   Nelson, D.L. Introduction to Spectroscopy. *Spectroscopic Methods in Food Analysis* **2017**, 3–33, doi:10.1201/B21879-2.

21.   Zhang, C.; Vinogradova, E. V.; Spokoyny, A.M.; Buchwald, S.L.; Pentelute, B.L. Arylation Chemistry for Bioconjugation. *Angewandte Chemie International Edition* **2019**, *58*, 4810–4839, doi:10.1002/anie.201806009.

22.   Acevedo, O.; Jorgensen, W.L. Solvent Effects and Mechanism for a Nucleophilic Aromatic Substitution from QM/MM Simulations. *Org Lett* **2004**, *6*, 2881–2884, doi:10.1021/ol049121k.

23.   Mayr, H. Modern Nucleophilic Aromatic Substitution. By Francois Terrier. *Angewandte Chemie International Edition* **2014**, *53*, 7119–7119, doi:10.1002/anie.201404183.

24.   Alapour, S.; Sharma, A.; de la Torre, B.G.; Ramjugernath, D.; Koorbanally, N.A.; Albericio, F. Perfluorophenyl Derivatives as Unsymmetrical Linkers for Solid Phase Conjugation. *Front Chem* **2018**, *6*, 1–10, doi:10.3389/fchem.2018.00589.

25.   Fox, M.A.; Pattison, G.; Sandford, G.; Batsanov, A.S. 19F and 13C GIAO-NMR Chemical Shifts for the Identification of Perfluoro-Quinoline and -Isoquinoline Derivatives. *J Fluor Chem* **2013**, *155*, 62–71, doi:10.1016/j.jfluchem.2013.05.005.

26.   Saunders, C.; Khaled, M.B.; Weaver, J.D.; Tantillo, D.J. Prediction of 19F NMR Chemical Shifts for Fluorinated Aromatic Compounds. *Journal of Organic Chemistry* **2018**, *83*, 3220–3225, doi:10.1021/acs.joc.8b00104.

27.   Siriwardana, K.; Wang, A.; Gadogbe, M.; Collier, W.E.; Fitzkee, N.C.; Zhang, D. Studying the Effects of Cysteine Residues on Protein Interactions with Silver Nanoparticles. *Journal of Physical Chemistry C* **2015**, *119*, 2910–2916, doi:10.1021/jp512440z.

28.   Miar, M.; Shiroudi, A.; Pourshamsian, K.; Oliaey, A.R.; Hatamjafari, F. Theoretical Investigations on the HOMO–LUMO Gap and Global Reactivity Descriptor Studies, Natural Bond Orbital, and Nucleus-Independent Chemical Shifts Analyses of 3-Phenylbenzo[d]Thiazole-2(3H)-Imine and Its Para-Substituted Derivatives: Solvent and Subs. *J Chem Res* **2021**, *45*, 147–158, doi:10.1177/1747519820932091.

29.   Anza, M.; Endale, M.; Cardona, L.; Cortes, D.; Eswaramoorthy, R.; Zueco, J.; Rico, H.; Trelis, M.; Abarca, B. Antimicrobial Activity, in Silico Molecular Docking, Admet and Dft Analysis of Secondary Metabolites from Roots of Three Ethiopian Medicinal Plants. *Advances and Applications in Bioinformatics and Chemistry* **2021**, *14*, 117–132, doi:10.2147/AABC.S323657.

30.   Salihović, M.; Pazalja, M.; Mahmutović-Dizdarević, I.; Jerković-Mujkić, A.; Suljagić, J.; Špirtović-Halilović, S.; Šapčanin, A. Synthesis, DFT Study and Antimicrobial Activity of Schiff Bases Derived from Benzaldehydes and Amino Acids. *Rasayan Journal of Chemistry* **2018**, *11*, 1074–1083, doi:10.31788/RJC.2018.1133077.

31. Parr, R.G.; Szentpály, L. v.; Liu, S. Electrophilicity Index. *J Am Chem Soc* **1999**, *121*, 1922–1924, doi:10.1021/JA983494X.

32. Abu-Melha, S. Design, Synthesis and DFT/DNP Modeling Study of New 2-Amino-5-Arylazothiazole Derivatives as Potential Antibacterial Agents. *Molecules* **2018**, *23*, 1–11, doi:10.3390/molecules23020434.

33. Lesjak, M.; Beara, I.; Simin, N.; Pintać, D.; Majkić, T.; Bekvalac, K.; Orčić, D.; Mimica-Dukić, N. Antioxidant and Anti-Inflammatory Activities of Quercetin and Its Derivatives. *J Funct Foods* **2018**, *40*, 68–75, doi:10.1016/j.jff.2017.10.047.

34. Boots, A.W.; Wilms, L.C.; Swennen, E.L.R.; Kleinjans, J.C.S.; Bast, A.; Haenen, G.R.M.M. In Vitro and Ex Vivo Anti-Inflammatory Activity of Quercetin in Healthy Volunteers. *Nutrition* **2008**, *24*, 703–710, doi:10.1016/j.nut.2008.03.023.

35. Miladiyah, I.; Jumina, J.; Haryana, S.M.; Mustofa, M. IN SILICO MOLECULAR DOCKING OF XANTHONE DERIVATIVES AS CYCLOOXYGENASE-2 INHIBITOR AGENTS. *Int J Pharm Pharm Sci* **2017**, *9*, 98, doi:10.22159/ijpps.2017v9i3.15382.

36. Rakesh, K.S.; Jagadish, S.; Balaji, K.S.; Zameer, F.; Swaroop, T.R.; Mohan, C.D.; Jayarama, S.; Rangappa, K.S. 3,5-Disubstituted Isoxazole Derivatives: Potential Inhibitors of Inflammation and Cancer. *Inflammation* **2016**, *39*, 269–280, doi:10.1007/s10753-015-0247-5.

37. López, R. Avogadro: An Advanced Semantic Chemical Editor, Visualization, and Analysis Platform. *J Cheminform* **2012**, *262*, 476–483, doi:10.1016/j.aim.2014.05.019.

38. Neese, F.; Wennmohs, F.; Becker, U.; Riplinger, C. The ORCA Quantum Chemistry Program Package. *Journal of Chemical Physics* **2020**, *152*, doi:10.1063/5.0004608.

39. Scott, A.P.; Radom, L. Harmonic Vibrational Frequencies: An Evaluation of Hartree-Fock, Møller-Plesset, Quadratic Configuration Interaction, Density Functional Theory, and Semiempirical Scale Factors. *Journal of Physical Chemistry* **1996**, *100*, 16502–16513, doi:10.1021/jp960976r.

40. Allouche, A. Software News and Updates Gabedit — A Graphical User Interface for Computational Chemistry Softwares. *J Comput Chem* **2012**, *32*, 174–182, doi:10.1002/jcc.

41. Teixeira, F.; Cordeiro, M.N.D.S. Improving Vibrational Mode Interpretation Using Bayesian Regression. *J Chem Theory Comput* **2019**, *15*, 456–470, doi:10.1021/acs.jctc.8b00439.

42. Saunders, C.; B. Khaled, M.; D. Weaver III, J.; J. Tantillo, D. Prediction of 19F NMR Chemical Shifts for Fluorinated Aromatic Compounds. *J Org Chem* **2018**, *83*, 3220–3225, doi:10.1021/acs.joc.8b00104.

43. P. Scott, A.; Radom, L. Harmonic Vibrational Frequencies: An Evaluation of Hartree−Fock, Møller−Plesset, Quadratic Configuration Interaction, Density Functional Theory, and Semiempirical Scale Factors. *J Phys Chem* **1996**, *100*, 16502–16513, doi:10.1021/jp960976r.

44. Abu-Melha, S. Design, Synthesis and DFT/DNP Modeling Study of New 2-Amino-5-Arylazothiazole Derivatives as Potential Antibacterial Agents. *Molecules* **2018**, *23*, 434, doi:10.3390/molecules23020434.

45. Trott, O.; Olson, A.J. AutoDock Vina: Improving the Speed and Accuracy of Docking with a New Scoring Function, Efficient Optimization and Multithreading. *J Comput Chem.* **2010**, *31*, 455–461, doi:10.1002/jcc.21334.

46. Seeliger, D.; de Groot, B.L. Ligand Docking and Binding Site Analysis with PyMOL and Autodock/Vina. *J Comput Aided Mol Des* **2010**, *24*, 417–422, doi:10.1007/s10822-010-9352-6.

47. C Reygaert, W. An Overview of the Antimicrobial Resistance Mechanisms of Bacteria. *AIMS Microbiol* **2018**, *4*, 482–501, doi:10.3934/microbiol.2018.3.482.

48. Allaka, T.R.; Katari, N.K.; Veeramreddy, V.; Anireddy, J.S. Molecular Modeling Studies of Novel Fluoroquinolone Molecules. *Curr Drug Discov Technol* **2018**, *15*, 109–122, doi:10.2174/1570163814666170829142044.

49. Shou, K.J.; Li, J.; Jin, Y.; Lv, Y.W. Design, Synthesis, Biological Evaluation, and Molecular Docking Studies of Quinolone Derivatives as Potential Antitumor Topoisomerase I Inhibitors. *Chem Pharm Bull (Tokyo)* **2013**, *61*, 631–636, doi:10.1248/cpb.c13-00040.

50. Narramore, S.; Stevenson, C.E.M.; Maxwell, A.; Lawson, D.M.; Fishwick, C.W.G. New Insights into the Binding Mode of Pyridine-3-Carboxamide Inhibitors of E. Coli DNA Gyrase. *Bioorganic and Medicinal Chemistry* **2019**, *27*, 3546–3550, doi:10.1016/j.bmc.2019.06.015.

51. Maghfiroh, K.; Widyarti, S.; Batoro, J.; Sumitro, S.B. Ethnopharmacological Study of Flavonoid Compounds in Magnolia Champaca (L.) Baill. Ex Pierre as Anti-Inflammatory Agents by Molecular Docking. *J Pharm Pharmacogn Res* **2021**, *9*, 584–597.